Azimuthal spectrum after parametric down-convertion with radial degrees of freedom

Yingwen Zhang[a], Filippus S. Roux[a], Melanie McLaren[a,b] and Andrew Forbes[a,b]

[a]CSIR National Laser Centre, PO Box 395, Pretoria 0001, South Africa;
[b]School of Physics, University of Witwatersrand, Johannesburg 2000, South Africa

ABSTRACT

Considering the quantum state produced in type I spontaneous parametric down-conversion with collinear, degenerate signal and idler beams, and a Gaussian pump, we show that the azimuthal Schmidt number in the Laguerre-Gaussian (LG) basis increases when the radial indices of the LG modes detected in the signal and idler beams are different. These observations are confirmed by the good agreement between theoretical and experimental results. The theoretical results are obtained by deriving expressions for the probability amplitude to detect LG modes with any combination of azimuthal and radial indices in a down-converted photonic quantum state.

Keywords: Quantum optic, Quantum state engineering and measurements, Spontaneous parametric down-conversion, Optical angular momentum, Entanglement production and manipulation

1. INTRODUCTION

Entanglement is a distinct phenomenon of quantum mechanics. A proper understanding and use of entanglement can lead to significant technological advances in communication, computing and cryptography.[1] In recent years there has been much interest in the entanglement among optical modes that carry orbital angular momentum (OAM).[2] These modes are capable of carrying large amounts of information due to the infinite-dimensional nature of OAM and thus are of significant interest for quantum information. Pairs of photons entangled in OAM can be readily produced through spontaneous parametric down-conversion (SPDC).[3–5] The degree of entanglement of a quantum state can be quantified by calculating the Schmidt number.[6] When restricted to the OAM degrees of freedom (by fixing the radial degrees of freedom) the equivalent quantity is called the azimuthal Schmidt number, which is also an indication of the width of the OAM spectrum, i.e. the spiral bandwidth.[6–10] Hence, a large spiral bandwidth indicates that an OAM entangled quantum state contains more OAM degrees of freedom that can be used to encode quantum information.

The Laguerre-Gaussian (LG) modes are OAM eigenstates and are a popular basis for photonic quantum information application. They also carry a radial index (p), which governs their radial dependence. It has been shown[6,11] that both azimuthal and radial degrees of freedom are required to saturate the full Schmidt number of a quantum state produced by SPDC. Nevertheless, the radial degrees of freedom are often neglected, summed over or fix to their simplest case $p = 0$. It has been shown that the azimuthal Schmidt number depends on the radial dependence of the chosen basis state and that the azimuthal Schmidt number obtained from Bessel-Gaussian (BG) modes, which are also OAM eigenstates, are larger than for LG modes.[12]

Here we investigate, theoretically and experimentally, how the azimuthal Schmidt number depends on the chosen radial dependence for an LG basis. For this purpose the radial indices are fixed to arbitrary values in the signal and idler beams, respectively. We restrict the analysis here to the case of degenerate collinear type I SPDC with a Gaussian pump. The results were also published in Ref. 13.

Further author information: (Send correspondence to Yingwen Zhang)
Yingwen Zhang: E-mail: YZhang@csir.co.za

Quantum Communications and Quantum Imaging XII, edited by Ronald E. Meyers, Yanhua Shih, Keith S. Deacon, Proc. of SPIE Vol. 9225, 92250D · © 2014 SPIE
CCC code: 0277-786X/14/$18 · doi: 10.1117/12.2063222

2. THEORY

2.1 Coincidence amplitude

The coincidence counts in a SPDC experiment are proportional to the modulus square of the down-converted probability amplitude, $|\mathcal{M}|^2 = |\langle \Psi_f | \mathcal{P} | \Psi_{in} \rangle|^2$, where $\mathcal{P}$ represents the SPDC process. For type I phase matching, with degenerate signal and idler frequencies ($\omega_\mathrm{s} = \omega_\mathrm{i} = \omega_\mathrm{d} = \omega_\mathrm{p}/2$) and collinear signal and idler beams, the probability amplitude in the paraxial limit is given by

$$\mathcal{M} \quad = \quad \Omega_0 \int M_\mathrm{s}^*(\mathbf{q}_1) M_\mathrm{i}^*(\mathbf{q}_2) M_\mathrm{p}(\mathbf{q}_1 + \mathbf{q}_2) S(\mathbf{q}_1 - \mathbf{q}_2) \, \frac{\mathrm{d}^2 q_1}{(2\pi)^2} \, \frac{\mathrm{d}^2 q_2}{(2\pi)^2} \tag{1}$$

where Ω_0 is an overall constant that determines the conversion efficiency, $\mathbf{q} = q_x \hat{x} + q_y \hat{y}$ is the two-dimensional transverse part of the three-dimensional wave-vector $\mathbf{k}$, the angular spectra of the mode profiles of the signal, idler and pump beams are given by $M_\mathrm{s}(\mathbf{q})$, $M_\mathrm{i}(\mathbf{q})$ and $M_\mathrm{p}(\mathbf{q})$, respectively, and $S(\mathbf{q}_1 - \mathbf{q}_2)$ is the phase matching function.

The pump beam is a Gaussian beam, so that

$$M_\mathrm{p}(\mathbf{q}) = \sqrt{2\pi} w_p \exp\left(-\frac{w_p^2}{4} |\mathbf{q}|^2 \right), \tag{2}$$

where w_p is the radius of the pump beam waist.

The signal and idler beam profiles are LG modes. Here we represent the angular spectra of these LG modes by

$$M_{\mathrm{s,i}}^{\ell,p}(\mathbf{q}) = \mathcal{N} \frac{1}{p!} \left[\partial_\eta^p \partial_\mu^{|\ell|} \mathcal{G} \right]_{\eta,\mu=0}, \tag{3}$$

where $\mathcal{G}$ is the generating function for the LG modes,[14] μ and η are generating parameters for the azimuthal and radial indices, respectively, and

$$\mathcal{N} = \left[\frac{2\pi 2^{|\ell|} p!}{(p + |\ell|)!} \right]^{1/2}. \tag{4}$$

The generating function is given by

$$\mathcal{G} \quad = \quad \frac{1}{1+\eta} \exp\left[\frac{\mathrm{i}(q_x \pm \mathrm{i} q_y) w \mu}{2(1+\eta)} - \frac{(q_x^2 + q_y^2) w^2 (1-\eta)}{4(1+\eta)} \right], \tag{5}$$

where w is the radius of the beam waists and the sign in the exponent is given by the sign of ℓ. For simplicity we assume that the radii of the beam waists of the signal and idler beams are equal $w_\mathrm{s} = w_\mathrm{i} = w$.

The phase matching function is given by

$$S(\mathbf{q}_1 - \mathbf{q}_2) = \mathrm{sinc}\left(\frac{\beta w_p^2}{8} |\mathbf{q}_1 - \mathbf{q}_2|^2 \right), \tag{6}$$

where we define $\mathrm{sinc}(a) = \sin(a)/a$ and β is a dimensionless combination of parameters. The latter is given by

$$\beta = \frac{n_o L \lambda_p}{\pi w_p^2} = \frac{n_o L}{z_R}, \tag{7}$$

where n_o is the ordinary refractive index of the nonlinear crystal, λ_p is the wavelength of the pump, L is the crystal length and z_R is the Rayleigh range.

The expression in Eq. (1) is a more general version of the integral considered previously.[9] Instead of setting the radial index to zero ($p = 0$) for both the signal and idler beams, we allow their radial indices to have arbitrary values. Using the generating function for LG modes, we are able to solve the more general integral analytically.

Evaluating the integral in Eq. (1), one finds that, unless the azimuthal indices of the signal and idler modes have equal magnitudes and opposite signs, the result is zero. One can therefore set $\ell_{\rm s} = -\ell_{\rm i} = \ell$. So we rewrite the generating function for explicit azimuthal indices, but leave the radial indices of the signal and idler beams implicit in terms of their generating parameters $\eta_{\rm s}$ and $\eta_{\rm i}$, respectively. The resulting generating function after integration is given by

$$\begin{aligned}\mathcal{G}_\ell &= \frac{{\rm i}\alpha^{|\ell|+1}}{\mathcal{B}^{|\ell|+1}\beta}\Big[Z^{|\ell|+1}\Phi(-Z,1,|\ell|+1) \\ &\quad -(Z^*)^{|\ell|+1}\Phi(-Z^*,1,|\ell|+1)\Big], \end{aligned} \tag{8}$$

where $\Phi(z,m,n)$ is the Lerch transcendent function,[15]

$$Z = \frac{(2-{\rm i}\beta)\mathcal{B}}{\alpha\mathcal{A}+{\rm i}\beta\mathcal{B}} \tag{9}$$

$$\mathcal{A} = (1-\eta_{\rm s})(1-\eta_{\rm i})\alpha + 2(1-\eta_{\rm s}\eta_{\rm i}) \tag{10}$$

$$\mathcal{B} = 2(1+\eta_{\rm s})(1+\eta_{\rm i}) + (1-\eta_{\rm s}\eta_{\rm i})\alpha \tag{11}$$

$$\alpha = \frac{w^2}{w_p^2}, \tag{12}$$

and β is defined in Eq. (7). Note that the generating parameters for the radial indices of the signal and idler beams are only found inside $\mathcal{A}$ and $\mathcal{B}$. To obtain the probability amplitude for particular radial indices p and q of the signal and idler beams, respectively, one evaluates the following operation

$$\mathcal{M} = \frac{\Omega_0}{w_p}\mathcal{N}_{pq}\left[\partial^p_{\eta_{\rm s}}\partial^q_{\eta_{\rm i}}\mathcal{G}_\ell\right]_{\eta_{\rm s},\eta_{\rm i}=0}, \tag{13}$$

where

$$\mathcal{N}_{pq} = \left[\frac{2(|\ell|!)^2}{\pi(p+|\ell|)!(q+|\ell|)!p!q!}\right]^{1/2}. \tag{14}$$

For the $p=0$ case, one sets $\eta_{\rm s}=\eta_{\rm i}=0$. As a result $\mathcal{A}=\mathcal{B}=2+\alpha$ and the expressions simplify to those obtained by Miatto, *et al.*[10]

2.2 Thin crystal limit

All the experimental parameters are contained in the dimensionless parameters α, Eq. (12), and β, Eq. (7). The latter is the ratio of the nonlinear crystal length L to the Rayleigh range of the pump beam z_R. In most practical experiments $L \ll z_R$. As a result $\beta \ll 1$. In this limit, the probability amplitude $\mathcal{M}$ can be expressed, to second order in β, as

$$\mathcal{M} = \frac{\Omega_0}{w_p}\mathcal{N}_{pq}\left(\frac{2}{\mathcal{A}}\right)^{|\ell|+1} + {\rm O}\left(\beta^2\right) \tag{15}$$

In the case where $\beta = 0$, the argument of the phase matching function in Eq. (6) becomes zero, with the result that the phase matching function is equal to 1. As a result, one can Fourier transform Eq. (1) to the coordinate domain. The result is a three-way overlap integral, given by

$$\mathcal{M} = \Omega_0 \int m_{\rm p}(\mathbf{x}) m_{\rm s}^*(\mathbf{x}) m_{\rm i}^*(\mathbf{x})\ {\rm d}^2x, \tag{16}$$

where $m_{\rm p,s,i}(\mathbf{x})$ represents the mode profile of the pump, signal or idler beam.

2.3 Schmidt number

To quantify the bandwidth of the spectrum of OAM modes we use the azimuthal Schmidt number, which is defined by

$$\kappa = \frac{1}{\sum_\ell P_\ell^2} \tag{17}$$

where P_ℓ represents the probability to observe a particular pair of OAM modes for a given set of p-indices. It is proportional to the modulus square of the probability amplitude. The coincidence counts $\mathcal{C}_\ell$ obtained in the experiment are proportional to the probabilities P_ℓ. Hence, the azimuthal Schmidt number can be computed by

$$\kappa = \frac{\left(\sum_\ell \mathcal{C}_\ell\right)^2}{\sum_\ell \mathcal{C}_\ell^2}. \tag{18}$$

3. EXPERIMENT

3.1 Experiment setup

The experimental setup is shown by the diagram in Fig. 1. A 350 mW pump laser with a wavelength of 355 nm traverses a 3 mm-thick BBO crystal to produce degenerate, collinear photon pairs with type I phase-matching, which are entangled in their OAM degrees of freedom. The beam size of the pump mode profile on the plane of the BBO is 1 mm. The signal and idler beams are separated using a 50/50 beam splitter. Each beam is directed onto a spatial light modulator (SLM) that is used to modulate the beam by the conjugate of the mode which is to be detected. Type-3 complex amplitude modulation given in[16] is used to generate the hologram on the SLMs, the LG mode size used on the hologram is 0.575 mm. The modulated beams are coupled into single mode fibres (SMFs), which extract the Gaussian profile from the beams. The beam size of the Gaussian mode of the SMF, imaged back onto the BBO crystal, is 0.575 mm. Avalanche photo diodes (APDs) that are connected to the other ends of these SMFs, register the photon pairs via a coincidence counter (CC).

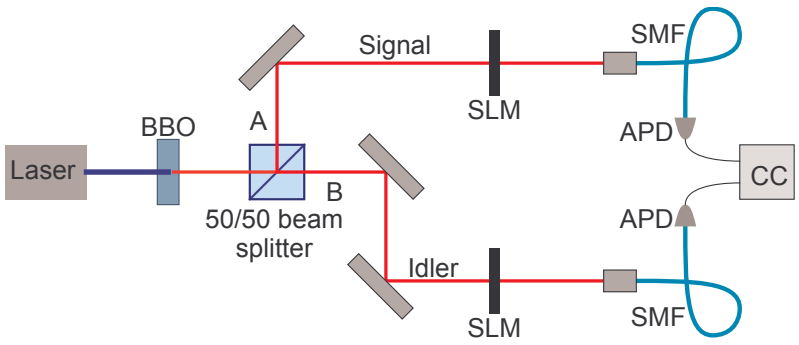

Figure 1. Diagram of the experimental setup used to prepare and measure the OAM entangled photon pairs.

3.2 Modelling the experiment

Due to the experimental parameters of the setup, $\beta = 0.0023$, which means that one can work in the thin crystal limit and use Eq. (16) to model the experiment. The SLMs are usually used to implemented the functions of $m_\mathrm{s}(\mathbf{x})$ and $m_\mathrm{i}(\mathbf{x})$, using complex amplitude modulation.[16] However, the coupling of the beams into the SMFs imply that the integrand must also contain the Gaussian modes of these SMFs. One can therefore express the actual overlap integral that is implemented by the experiment as

$$\mathcal{M} = \Omega_0 \int m_\mathrm{p}(\mathbf{x}) m_\mathrm{s}^*(\mathbf{x}) m_\mathrm{i}^*(\mathbf{x}) G^2(\mathbf{x})\ \mathrm{d}^2x, \tag{19}$$

where

$$G(\mathbf{x}) = \left(\frac{2}{\pi}\right)^{1/2} \frac{1}{w_0} \exp\left(-\frac{x^2+y^2}{w_0^2}\right) \tag{20}$$

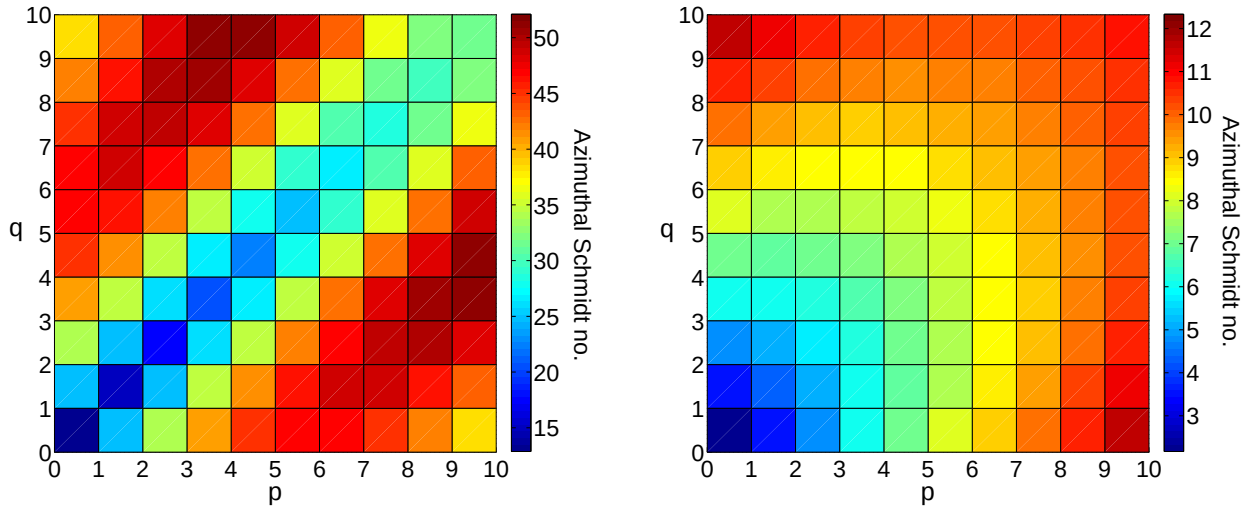

(a) (b)

Figure 2. Intensity plot of the azimuthal Schmidt number κ calculated using Eq. (16) for p, q running from 0 to 10 showing the difference before and after the SMF Gaussian profiles are taken into account. (a) shows the Schmidt numbers calculated without taking into account the SMF Gaussians and (b) with the SMF Gaussians. The parameters used here for the calculations are the same as the experimental parameters namely $w_p = 1$ mm, $w = 0.575$ mm and $w_0 = 0.575$ mm giving $\alpha = 0.331$ for (a) and $\alpha = 2.34$ for (b).

is the mode of the SMF, with radius w_0 when imaged onto the nonlinear crystal. Since the pump is also a Guassian function, the effect of these extra Gaussian functions is to modify the effective mode size of the pump

$$\exp\left(-\frac{x^2+y^2}{w_p^2}\right) \to \exp\left(-\frac{x^2+y^2}{(w_p')^2}\right), \tag{21}$$

where

$$\frac{1}{(w_p')^2} = \frac{1}{w_p^2} + \frac{2}{w_0^2}. \tag{22}$$

The effective mode size of the pump is smaller than the mode size of the original pump beam. To take the effect of the SMF Gaussian profiles into account in the theory, one merely needs to replace $w_p \to w_p'$ in the expressions in Sec. 2. It was found that if one does not take the effect of these SMF Gaussian profiles into account, the theoretical results differ significantly from the experimental results as can be seen in Fig. 2, which shows the azimuthal Schmidt number κ calculated theoretically before and after the SMF Gaussians has been taken into account.

One could in principle modify the modes on the SLMs to compensate for the extra Gaussian profiles coming from the SMFs. However, in practice this can only work if the radial functions of the modes on the SLMs are scale invariant, as in the case of the LG modes with $p = 0$.

3.3 Experimental results

Figure 3 (a) shows an intensity plot of κ measured experimentally for p and q combinations running from 0 to 5. The diagonals of Fig. 3 (a) are shown in Fig. 3 (b) and (c) which also compares the experimentally measured κ to that determined theoretically. From Fig. 3 it can be seen that κ increases with larger p and q values and also when $|p-q|$ grows larger.

In general the experimental results agrees with theory, however, in Fig. 3 (b) one sees that the errors in the data grows very large at large $|p-q|$, and in Fig. 3 (c) the growth in κ with p for the experimental results is slightly slower than that of the theoretical. These effects can be explained if one take a look at Fig. 4 which shows

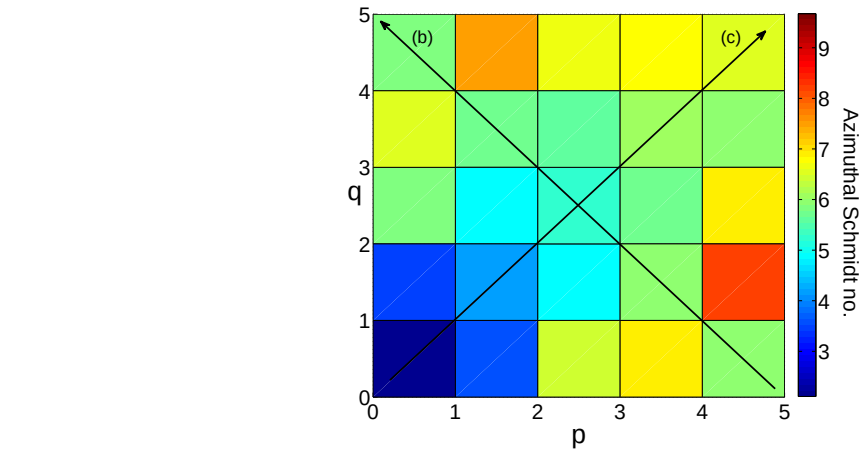

(a)

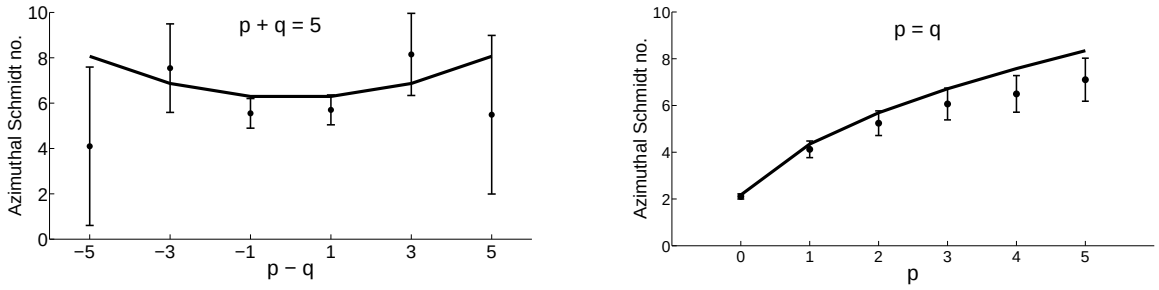

(b) (c)

Figure 3. (a) Intensity plot of the azimuthal Schmidt number κ determined experimentally for radial indices p and q running from 0 to 5. (b) and (c) shows the experimental results (dots) compared to the theoretical results (line) along the diagonals indicated by the arrows in (a). Error bars corresponds to one standard deviation.

the intensity graphs of the experimentally measured coincidence count rate $\mathcal{C}_\ell$ (Fig. 4 (a)), and the normalized probability amplitude P_ℓ determined theoretically (Fig. 4 (b)) at $\ell = 5$.

One sees in Fig. 4 (a) that $\mathcal{C}_\ell$ is small when $|p-q|$ is large, in fact it never exceeded 3 counts per second (with background subtracted) at the two corners where $|p-q| = 5$ for any ℓ's. This results in the very large error bars seen in Fig. 3 (b). Apart from the increase in the size of the error bars, we also see a larger disagreement between theory and measured results at the end points of the curve in Fig. 3(c). This disagreement is believed to be caused by a reduced fidelity of the modal function on the SLM when using intensity masking to represent the mode. Due to the limited resolution of the SLM, modal functions with larger p and ℓ indices are rendered with less accuracy, compared to those with smaller p and ℓ indices.

From the above results, we see that, with our experimental parameters, the combination of radial indices that gives the optimal spiral bandwidth, while maintaining good beam quality and acceptable coincidence count rates, are for p and q equal to 1 and 3 (or 3 and 1). The resulting value of the azimuthal Schmidt number κ is approximately 3 times that at $p = q = 0$.

4. CONCLUSION

The effect of the radial index of the LG basis on the spiral (OAM) bandwidth of down-converted photon states were investigated. It is shown, both theoretically and experimentally, that, when the radial index of the signal and idler beams are different, the spiral bandwidth tends to increase. In other words, although the diagonal modes (those with the same radial indices for the signal and idler beams) are dominant, the off-diagonal modes give

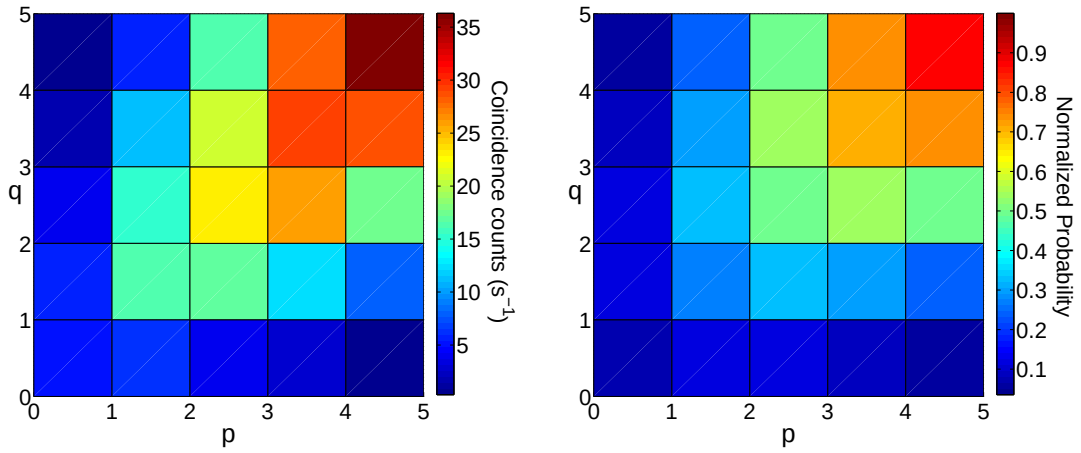

(a) (b)

Figure 4. (a) Coincidence count rate $\mathcal{C}_\ell$ measured experimentally and (b) normalized probability amplitude P_ℓ determined theoretically for p and q running from 0 to 5 with $\ell = 5$.

larger spiral bandwidths. The experimental setup in this case employs type I SPDC with collinear, degenerate signal and idler beams, and a Gaussian pump.

For the purpose of the theoretical analysis we obtained analytic expressions for the probability amplitude to detect photon pairs with arbitrary LG modes. Using generating functions for the LG modes, we were able to obtain expressions that apply for any combination of azimuthal and radial indices. For the case when the radial indices are set to zero, our expressions agree with those found in previous work.[5,9,10]

Using these expressions we calculated the azimuthal Schmidt number for different combinations of signal and idler beam radial indices and compared them with the experimentally measured azimuthal Schmidt numbers. The agreement between theory and experiment is fairly good provided the radial indices are not too large ($p \lesssim 5$) and the difference between the signal and idler radial index is small ($|p - q| \lesssim 3$). We also demonstrated that it is possible to obtain up to a threefold increase in the azimuthal Schmidt number without a significant loss in coincidence count rate.

To be able to model the experimental setup accurately it is also important that the effect of the Gaussian modes of the SMFs are taken into account in the overlap integral.

REFERENCES

[1] Nielsen, M. A. and Chuang, I. L., [*Quantum computation and quantum information*], Cambridge University Press, New York (2010).

[2] Jack, B., Yao, A. M., Leach, J., Romero, J., Franke-Arnold, S., Ireland, D. G., Barnett, S. M., and Padgett, M. J., "Entanglement of arbitrary superpositions of modes within two-dimensional orbital angular momentum state spaces," *Phys. Rev. A* **81**, 043844 (2010).

[3] Mair, A., Vaziri, A., Weihs, G., and Zeilinger, A., "Entanglement of the orbital angular momentum states of photons," *Nature* **412**, 313–316 (2001).

[4] Franke-Arnold, S., Barnett, S. M., Padgett, M. J., and Allen, L., "Two-photon entanglement of orbital angular momentum states," *Phys. Rev. A* **65**(3), 033823 (2002).

[5] Torres, J. P., Alexandrescu, A., and Torner, L., "Quantum spiral bandwidth of entangled two-photon states," *Physical Review A* **68**, 050301 (2003).

[6] Law, C. K. and Eberly, J. H., "Analysis and interpretation of high transverse entanglement in optical parametric down conversion," *Phys. Rev. Lett.* **92**, 127903 (2004).

[7] Molina-Terriza, G., Torres, J. P., and Torner, L., "Management of the angular momentum of light: Preparation of photons in multidimensional vector states of angular momentum," *Phys. Rev. Lett.* **88**, 013601 (2001).

[8] Pors, B.-J., Monken, C. H., Eliel, E. R., and Woerdman, J. P., "Transport of orbital-angular-momentum entanglement through a turbulent atmosphere," *Opt. Express* **19**, 6671–6683 (2011).

[9] Miatto, F. M., Yao, A. M., and Barnett, S. M., "Full characterization of the quantum spiral bandwidth of entangled biphotons," *Phys. Rev. A* **83**, 033816 (2011).

[10] Miatto, F. M., Giovannini, D., Romero, J., Franke-Arnold, S., Barnett, S. M., and Padgett, M. J., "Bounds and optimisation of orbital angular momentum bandwidths within parametric down-conversion systems," *Eur. Phys. J. D* **66**, 1–6 (2012).

[11] Salakhutdinov, V., Eliel, E., and Löffler, W., "Full-field quantum correlations of spatially entangled photons," *Phys. Rev. Lett.* **108**, 173604 (2012).

[12] McLaren, M., Agnew, M., Leach, J., Roux, F. S., Padgett, M. J., Boyd, R. W., and Forbes, A., "Entangled bessel-gaussian beams," *Opt. Express* **20**, 23589–23597 (2012).

[13] Zhang, Y., Roux, F. S., McLaren, M., and Forbes, A., "Radial modal dependence of the azimuthal spectrum after parametric down-conversion," *Phys. Rev. A* **89**, 043820 (2014).

[14] Roux, F. S., "Infinitesimal-propagation equation for decoherence of an orbital-angular-momentum-entangled biphoton state in atmospheric turbulence," *Phys. Rev. A* **83**, 053822 (2011).

[15] Jeffrey, A. and Zwillinger, D., [*Table of Integrals, Series, and Products*], Elsevier Science (2007).

[16] Arrizón, V., Ruiz, U., Carrada, R., and González, L. A., "Pixelated phase computer holograms for the accurate encoding of scalar complex fields," *J. Opt. Soc. Am. A* **24**, 3500–3507 (2007).